



OPEN ACCESS

EDITED BY

Jing Wei,
Sun Yat-sen University, China

REVIEWED BY

Anirban Chakraborty,
Idaho State University, United States
Alberto Sánchez-González,
Instituto Politécnico Nacional
(IPN), Mexico

*CORRESPONDENCE

Hong-Chun Li
hcli1960@ntu.edu.tw

†These authors have contributed
equally to this work

SPECIALTY SECTION

This article was submitted to
Marine Biogeochemistry,
a section of the journal
Frontiers in Marine Science

RECEIVED 30 June 2022

ACCEPTED 10 August 2022

PUBLISHED 02 September 2022

CITATION

Xu H, Li D-W, Li H-C, Zhao M,
Berelson WM, Jin G'e, Li L and Misra S
(2022) Local and remote forcing on
the interannual variations of the
sedimentary $\delta^{15}\text{N}$ in Santa Barbara
Basin during the past 80 years.
Front. Mar. Sci. 9:982051.
doi: 10.3389/fmars.2022.982051

COPYRIGHT

© 2022 Xu, Li, Li, Zhao, Berelson, Jin, Li
and Misra. This is an open-access article
distributed under the terms of the
[Creative Commons Attribution License
\(CC BY\)](https://creativecommons.org/licenses/by/4.0/). The use, distribution or
reproduction in other forums is
permitted, provided the original
author(s) and the copyright owner(s)
are credited and that the original
publication in this journal is cited, in
accordance with accepted academic
practice. No use, distribution or
reproduction is permitted which does
not comply with these terms.

Local and remote forcing on the interannual variations of the sedimentary $\delta^{15}\text{N}$ in Santa Barbara Basin during the past 80 years

Hanyue Xu^{1,2†}, Da-Wei Li^{1,2†}, Hong-Chun Li^{1,3*}, Meixun Zhao^{1,2}, William M. Berelson⁴, Gui'e Jin¹, Li Li¹ and Satabdi Misra³

¹Frontiers Science Center for Deep Ocean Multispheres and Earth System, and Key Laboratory of Marine Chemistry Theory and Technology, Ministry of Education, Ocean University of China, Qingdao, China, ²Laboratory for Marine Ecology and Environmental Science, Qingdao National Laboratory for Marine Science and Technology, Qingdao, China, ³Department of Geosciences, National Taiwan University, Taipei, Taiwan, ⁴Department of Earth Sciences, University of Southern California, Los Angeles, CA, United States

Sedimentary nitrogen isotope ($\delta^{15}\text{N}_{\text{sed}}$) in Santa Barbara Basin (SBB) has been mostly interpreted as the record of the eastern tropical North Pacific (ETNP) intermediate water denitrification process. Nevertheless, debate remains regarding sources and control mechanisms of $\delta^{15}\text{N}_{\text{sed}}$ signal in SBB. Multi-proxy analyses including $\delta^{15}\text{N}_{\text{sed}}$, total organic carbon (TOC), total nitrogen (TN), C/N ratio, and marine biomarkers were performed on a 46-cm sediment core (SBB-190629) collected from SBB in 2019. The core was dated with varve counting and ²¹⁰Pb dating method, showing a depositional history of 1938–2019 CE with a sedimentation rate of 0.564 cm/year. The findings show that the $\delta^{15}\text{N}_{\text{sed}}$ record (at ~0.25-year resolution) ranges from 6.24‰ to 7.43‰, which was affected by both local and remote forcing. The long-term variations of the SBB $\delta^{15}\text{N}_{\text{sed}}$ signature show a general decreasing trend from 1940 to the late 1980s, low values during 1980~2000, and an increase afterward, which is thought to reflect changes in ETNP denitrification induced by the strength of tropical trade winds. Our results also reveal a series of abrupt annual to multiannual changes, superimposed on the long-term variation mentioned above. The SBB local $\delta^{15}\text{N}$ signal ($\Delta\delta^{15}\text{N}_{\text{SBB}}$) is accessed by using the deviation from the mean $\delta^{15}\text{N}$ ($\Delta\delta^{15}\text{N}$) of SBB-190629 to subtract the $\Delta\delta^{15}\text{N}$ of the ETNP. The $\Delta\delta^{15}\text{N}_{\text{SBB}}$ record compares well with redox-sensitive proxies (Re/Mo ratio and C₂₉ stanol/stenol ratio) from the SBB bottom water and with the OC_{marine} content calculated based on the C/N ratio mixing model, indicating that the $\Delta\delta^{15}\text{N}_{\text{SBB}}$ is mainly controlled by bottom water denitrification, which was induced by the change of upwelling intensity and marine productivity. Since

various climatic factors (e.g., El Niño–Southern Oscillation (ENSO), Pacific Decadal Oscillation (PDO), and North Pacific Gyre Oscillation (NPGO)) have different impacts on the upwelling intensity (hence the marine productivity and denitrification) in SBB on different timescales, the influence of combined climatic factors on SBB denitrification is time dependent.

KEYWORDS

$\delta^{15}\text{N}_{\text{sed}}$ variation, denitrification, Santa Barbara Basin, climatic forcing, Eastern Tropical Northern Pacific ventilation

1 Introduction

In a marine system under oxygen-deficient conditions, e.g., eastern tropical North Pacific (ETNP), microbial activity converts bioavailable nitrate (NO_3^-) to nitrogen (N_2) via the denitrification process. The intensity of the oxygen-deficient zone (ODZ) controls water column denitrification, as nitrate becomes the favorable electron acceptor after dissolved O_2 is exhausted during microbially regulated organic carbon (OC) remineralization (Altabet et al., 1999; Ward, 2011; Horak et al., 2016; Margolskee et al., 2019). During the denitrification process, ^{14}N is preferentially removed from the water column, and ^{15}N is progressively enriched in the remaining nitrate pool (Altabet, 2006; Davis et al., 2019; Wang et al., 2019). Therefore, with a stronger ODZ, the water column denitrification is stronger, which creates a more positive $\delta^{15}\text{N}$ of the water column. The $\delta^{15}\text{N}_{\text{nitrate}}$ -enriched water from the ODZ is upwelled into the photic zone and incorporated into phytoplankton. After the death of the phytoplankton, the organic matter with a high $\delta^{15}\text{N}$ signal via sinking particles is preserved in the marine sediment (Rayner et al., 2003; Wang et al., 2019). Under the circumstance of complete nitrate utilization (biological fractionation effects are negligible) and the absence of sedimentary diagenesis, such changes can be recorded in marine sedimentary $\delta^{15}\text{N}$ ($\delta^{15}\text{N}_{\text{sed}}$) (Altabet et al., 1999; Emmer and Thunell, 2000; Thunell and Kepple, 2004; Ward, 2011; Horak et al., 2016; Davis et al., 2019; Margolskee et al., 2019; Wang et al., 2019; Sánchez et al., 2022). Hence, in regions where these conditions are met, $\delta^{15}\text{N}_{\text{sed}}$ is accepted as a proxy for the integrated rates of denitrification and the volume of the ODZ: when the ODZ is expanded and the water column denitrification is intensified, the $\delta^{15}\text{N}_{\text{sed}}$ increases (Emmer and Thunell, 2000; Tems et al., 2015; Horak et al., 2016; Davis et al., 2019; Wang et al., 2019; Sánchez et al., 2022).

Santa Barbara Basin (SBB; Figure 1A) is located between the California Coast to the north and the Channel Islands to the south, particularly in the Southern California Bight (Emmer and Thunell, 2000; Hendy et al., 2015; Osborne et al., 2016; Davis et al., 2019; Wang et al., 2019). It is a shallow nearshore basin

with a maximum depth of ~600 m. The basin is bordered with narrow sills to the west (~475-m depth) and east (~230-m depth), which further reduces ventilation combined with the re-mineralization of organic matter, creating an anoxic water environment (dissolved oxygen < 0.1 ml/L) below the sills (Emmer and Thunell, 2000; Bograd et al., 2002; Goericke et al., 2015). The high sedimentation rate and anoxic depositional environment minimize bioturbation, creating high-resolution and low sedimentary diagenesis records in SBB (Hendy et al., 2015; Sarno et al., 2020). A minimal (<1‰) offset between the sediment trap $\delta^{15}\text{N}$ time series and down core $\delta^{15}\text{N}_{\text{sed}}$ records in SBB provides further support that diagenetic isotopic alteration on $\delta^{15}\text{N}_{\text{sed}}$ is negligible (Altabet et al., 1999; Emmer and Thunell, 2000; Davis et al., 2019; Wang et al., 2019). Furthermore, previous studies show that nitrogen utilization is complete in SBB surface waters throughout the year except in spring. During the spring, a large amount of nutrients is brought by upwelling, which may affect nitrogen utilization in the surface water. However, all of the upwelled nitrate is completely utilized on interannual scales (Emmer and Thunell, 2000; Davis et al., 2019). Therefore, $\delta^{15}\text{N}_{\text{sed}}$ from the SBB records the variation of $\delta^{15}\text{N}$ in the water column and is a good potential indicator of changes in ODZs and water column denitrification on longer than annual scales in the past.

The $\delta^{15}\text{N}$ (and $\delta^{15}\text{N}_{\text{sed}}$) value of the water column (sediment) in SBB is affected by several factors. In near-surface circulation (upper 100 m) of SBB, the interaction between the cold southward flowing California Current (CC) and relatively warm northward flowing countercurrents (Davidson current) creates a semi-permanent cyclonic gyre. Annual variations in the strength of the two surface currents under climatic forcing such as El Niño/La Niña and Pacific Decadal Oscillation (PDO) strongly affect the degree of upwelling, thermocline depth, and biological productivity within the basin and in turn influence water column denitrification and $\delta^{15}\text{N}$ value (Liu and Kaplan, 1989; Tems et al., 2015; Davis et al., 2019; Wang et al., 2019). Between depths of 100 and 400 m, the highly saline, anoxic, and $\delta^{15}\text{N}$ -enriched waters originating from the ETNP zone are deflected to SBB through the California Undercurrent (CUC)

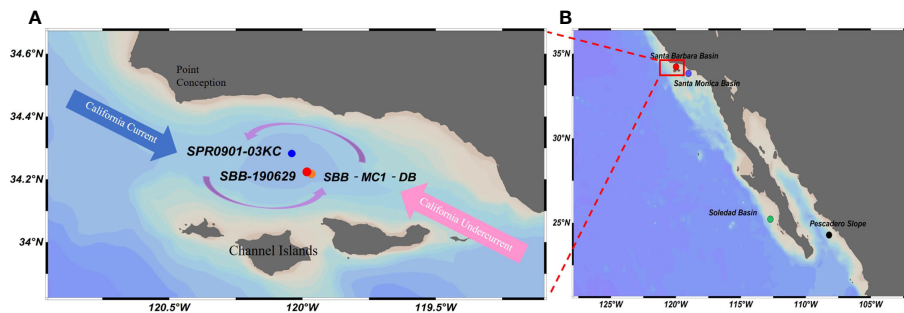


FIGURE 1

(A) Map of Santa Barbara Basin and the surrounding region, showing sampled and referred core locations in Santa Barbara Basin (SBB). Red circle (●), core SBB-190629 (this study); blue circle (●), core SPR0901-03KC from Wang et al. (2019); orange circle (●), core SBB-MC1-DB from Davis et al. (2019). Major currents are mentioned in the text. (B) Locations of core sites along the North American margin are referred to in this study. Red circle (●), Santa Barbara Basin core location in this study. Purple circle (●), Santa Monica Basin core location from Davis et al. (2019). Green circle (●), Soledad Basin core location from Deutsch et al. (2014). Black circle (●), Pescadero Slope core location from Deutsch et al. (2014). Red box indicates SBB region and is enlarged in panel A.

(Figure 1A). The ETNP has the largest volume of low- O_2 waters of all ODZs along the equator to mid-latitude in the northeastern Pacific (Horak et al., 2016); fluctuations of the intensity of denitrification in the ETNP are reflected on water $\delta^{15}N$ and advected to SBB. Compared with the denitrified water from ETNP, CC input with lower $\delta^{15}N$ is considered a relatively stable end-member on decadal scales in the nitrogen isotopic mass balance of the SBB input water. Therefore, in this study, the ETNP $\delta^{15}N$ variation represents the distal signal (or remote forcing) in SBB $\delta^{15}N$ budget. Finally, the SBB bottom waters (>475 m) are derived from North Pacific Intermediate Water (NPIW), which periodically flows over the deepest sill and further complicates the water column oxygen content and denitrification in SBB.

Previous studies have focused on the SBB $\delta^{15}N_{sed}$ records as the distal signal of ETNP denitrification. However, some studies show that variation of $\delta^{15}N_{sed}$ in SBB is associated not only with the change of ETNP ODZ but also with oxygen loss along the California Margin (Liu and Kaplan, 1989; Emmer and Thunell, 2000; Deutsch et al., 2014; Tems et al., 2015; Davis et al., 2019). In the study of Davis et al. (2019), the $\delta^{15}N_{sed}$ record of core SBB-MC1-DB (Figure 1A) covering a sedimentary history of 1892–2017 CE was used to examine the decadal-scale variability (via Walker Circulation) and long-term anthropogenic forcing to $\delta^{15}N$ signals; the difference of $\delta^{15}N_{sed}$ between ETNP and SBB was the result of anthropogenic forced changes; however, factors of regional oceanography may be a candidate but ignored. Wang et al. (2019) combined $\delta^{15}N_{sed}$ records (SPR0901-03KC in Figure 1A) of the SBB with additional productivity proxies to assess local and remote forcing of denitrification in the Northeast Pacific for the last 2,000 years. They suggest that wind curl upwelling (local signal) contributes to Southern California's primary productivity and denitrification process, especially during weak coastal upwelling intervals. However,

the resolution and chronological coverage of the core SPR0901-03KC $\delta^{15}N_{sed}$ record was not able to compare with instrumental climatic records. Furthermore, recent studies have identified an increase in water column denitrification in the bottom waters of SBB (Goericke et al., 2015; White et al., 2019), and the $\delta^{15}N$ signal could be transported into the upper water column *via* eddy diffusion and upwelling. Hence, understanding of $\delta^{15}N$ variation on annual-to-decadal timescales and its influencing factors in SBB requires further investigation.

The present study aims to detect the local $\delta^{15}N$ signal from the $\delta^{15}N_{sed}$ record and understand the role of climatic fluctuations and oceanic upwelling on interannual $\delta^{15}N$ variations in SBB. To do this, a 46-cm-long sediment core spanning 80 years of depositional history was sampled at a high resolution (every ~0.25 years) and analyzed for nitrogen isotopic signature. The local $\delta^{15}N$ signals are separated from the bulk $\delta^{15}N_{sed}$ throughout the comparison with the distal $\delta^{15}N$ signals of the ETNP denitrification records published in the previous literature. Then, the variation of the SBB local $\Delta\delta^{15}N$ ($\Delta\delta^{15}N_{SBB}$) signals is compared with several geochemical parameters $\{(Re/Mo)_{EF}$, C_{29} stanol/stenol ratio, marine OC, marine biomarkers} to understand changes in redox condition, O_2 content, and productivity in SBB. The role of climatic indices such as PDO, North Pacific Gyre Oscillation (NPGO), and El Niño–Southern Oscillation (ENSO) as influencing factors in shaping $\delta^{15}N_{sed}$ signatures of the SBB is comprehensively discussed.

2 Methods

2.1 Core SBB-190629 and sampling

Core SBB-190629 (34°13.4'N, 119°58.99'W; 583-m depth) was collected on board the *RV Oceanus* by a multi-core device

from SBB on 29 June 2019. The core was 46 cm long and contained clear laminations (Figure 2A). It was split in half and kept in a cold room at 4°C in the Department of Earth Sciences at the University of Southern California (USC). Half of the core was transported to the Department of Geosciences at the National Taiwan University (NTU) in February 2020. During the transportation, the sediments were contracted from 46 to 35 cm. Therefore, sampling depths were calibrated back to the original depths (Figure 2B). In Figure 2A, the depth scale of the core was the original depth. In Figure 2B, the depth scale of the core was the depth of the core at sampling time. The original depth of the core changed from 46 to 35 cm after the contraction. However, the main features of the color changes in the core sediments remained. Therefore, the depth correlations were able to be established (see the dashed lines in Figures 2A, B). With the correlated controlling depths, the relationship between sampling depth (D_1) and original depth (D_0) was $D_1 = 0.1408 + 0.6193 \times D_0 + 0.0037 \times D_0^2$ ($R^2 = 1.00$).

The half core was subsampled at a 1-cm interval for ^{210}Pb dating and biomarker analysis and then subsampled at a 2–3-mm interval (roughly four samples within 1 cm) for fine-resolution total organic carbon (TOC), total nitrogen (TN), and $\delta^{15}\text{N}$ analyses. A total of 160 subsamples had been obtained. All sediment samples were freeze-dried by a freeze vacuum dryer (model EYELA FDU-1200), then ground, and mixed well. All dried samples were stored in a refrigerator at 8°C until analysis.

2.2 ^{210}Pb dating

A total of 22 horizons of the core were analyzed for ^{210}Pb dating through a high-resolution ORTEC GEM-FX8530P4 gamma spectrometer with a 10-cm-thick low-background lead shield in the NTUAMS Lab at NTU. The energy of ^{210}Pb , ^{226}Ra , ^{214}Pb , and ^{214}Bi peaks in the gamma spectrometer was at 46, 186, 351, and 610 keV, respectively. Each dry sample (weighing ranging from 5 to 10 g) in a plastic sample container was placed on top of the detector. Counting efficiency, geometry, and density effects of the detector were calibrated by various standards. Supported ^{210}Pb activity was determined by either the ^{226}Ra activity or activity of $(^{214}\text{Pb} + ^{214}\text{Bi})/2$ in the sample measurements (Li et al., 2019). The excess ^{210}Pb equals total ^{210}Pb activity minus either ^{226}Ra activity or activity of $(^{214}\text{Pb} + ^{214}\text{Bi})/2$. The results are shown in Figure 2C and listed in Supplementary Table S1.

2.3 Total organic carbon, total nitrogen, and $\delta^{15}\text{N}$ analysis

Sediment samples were taken at 2–3-mm intervals for TOC, TN, and $\delta^{15}\text{N}$ analyses. The samples were treated with 0.5 mol/L of HCl for removal of carbonates and subsequently rinsed with Milli-Q water repeatedly until a pH of 7 was reached. After that, the samples were centrifuged to remove water and then oven-dried at 50°C for 48 h. Then, a small amount (approximately 5–10 mg) of

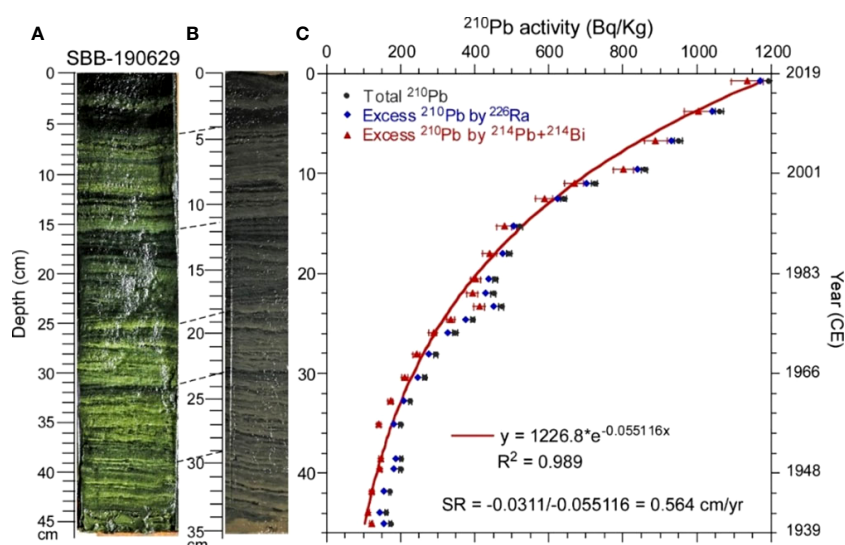


FIGURE 2

Photos and ^{210}Pb profile of core SBB-190629. (A) Photo of the core before transportation to National Taiwan University (NTU). (B) Photo of the core after transportation to NTU. (C) ^{210}Pb profile. The constructed ages are shown on the right-hand side of the plot. Red line represents the fitting curve.

samples were taken and placed in a tinfoil boat and analyzed for TOC and TN contents with an Elemental Analyzer FLASH 2000 at Ocean University of China (OUC) with a standard deviation of ± 0.02 wt.% ($n = 6$), determined by replicate analysis of atropine (Thermo Fisher Scientific, Breda, Netherlands) and a low organic content soil (Elemental Microanalysis Ltd., Okehampton, UK). Other 0.5–1 mg samples were placed in a tinfoil boat and analyzed for $\delta^{15}\text{N}$ on EA-IRMS (FLASH EA 1112 series coupled with Thermo Fisher Delta V continuous flow isotopic ratio mass spectrometer) at OUC. Measured $\delta^{15}\text{N}$ values were calibrated against nitrogen isotope standards N-1 ($\delta^{15}\text{N} = 0.40\text{‰}$) and USGS-40 ($\delta^{15}\text{N} = -4.52\text{‰}$).

$$\delta^{15}\text{N} = \left[\left(\frac{{}^{15}\text{N}/{}^{14}\text{N}_{\text{sample}}}{{}^{15}\text{N}/{}^{14}\text{N}_{\text{standard}}} \right) - 1 \right] \times 1,000 \quad (1)$$

The precision of the $\delta^{15}\text{N}$ measurements is reflected by the standard deviation of the duplicated N-1 and USGS-40 measurements, which is less than $\pm 0.10\text{‰}$ ($n = 6$). The results

of TOC, TN, and $\delta^{15}\text{N}$ are shown in Figure 3 and listed in Supplementary Table S2.

2.4 Biomarker analysis

Total lipids were extracted from freeze-dried sediment samples (0.15–0.25 g) by using a dichloromethane and methanol (3:1 v/v) mixture utilizing ultrasonication (15 min). After that, an internal standard mixture containing C_{19} *n*-alkanol and *n*- $\text{C}_{24}\text{D}_{50}$ was added to the samples. The total lipid extracts were extracted by centrifuge. The extracts were then hydrolyzed with 6% KOH in MeOH. The non-polar lipid fractions were eluted with 8 ml of hexane using silica gel chromatography and then subsequently dried under a gentle N_2 stream. The alcohol lipid fractions (containing marine phytoplankton biomarkers) were further eluted with 12 ml of

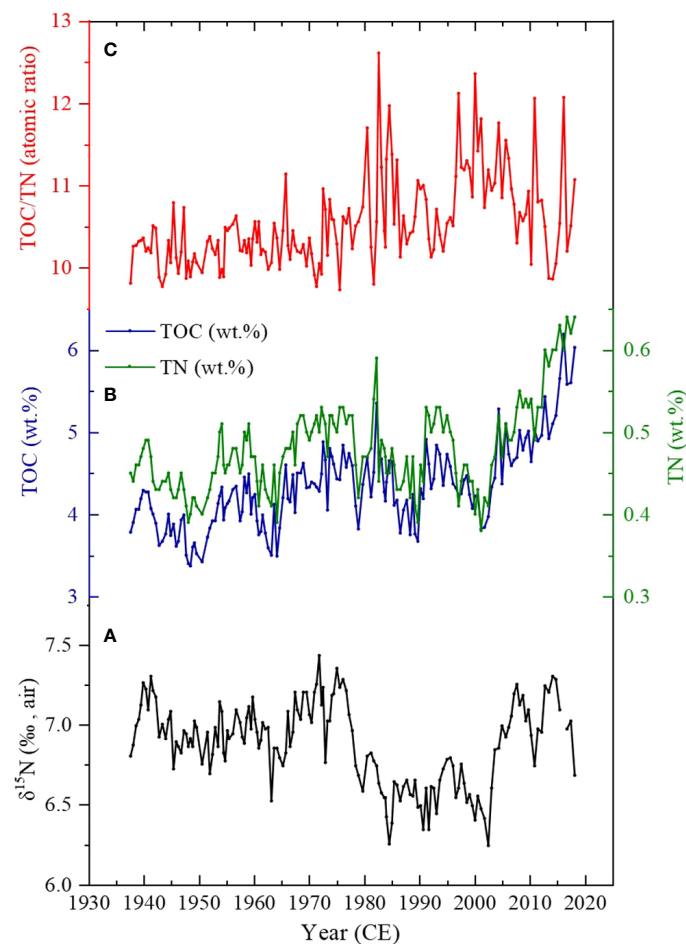


FIGURE 3
TOC, TN, and $\delta^{15}\text{N}$ variation of the core SBB-20190629. (A) $\delta^{15}\text{N}$ variation in core SBB-190629. (B) Total organic carbon (TOC, wt.%) and total nitrogen (TN, wt.%) records from SBB-20190629. (C) C/N atomic ratio (atom ratio of TOC/TN).

dichloromethane and methanol (95:5, v/v), dried under a gentle N_2 stream, and derivatized using *N,O*-bis(trimethylsilyl)-trifluoroacetamide (BSTFA) at 70°C for 1 h before instrumental measurements. Biomarker quantification was performed on an Agilent 6890N GC with a flame ionization detector (FID) (Li et al., 2014). The biomarker contents were plotted in Figure 4A and listed in Supplementary Table S3.

2.5 Data processing and sources

Ancillary hydrologic data over the period 1953–2018 CE were collected from the California Cooperative Oceanic Fisheries Investigations program (CalCOFI) as described at <http://calcofi.org>. Determinations as to the phase and state of PDO were available at <http://jisao.washington.edu/pdo/PDO>. The climate indices of ENSO represented by the Niño 3.4 region (5°N–5°S, 170°W–120°W) are available at https://www.esrl.noaa.gov/psd/gcos_wgsp/Timeseries/. The NPGO index by Di Lorenzo et al. (2008) is available at <http://www.o3d.org/npgo/>.

2.6 Statistics

The temporal changes of TOC, TN, and $\delta^{15}N$ over time were assessed using the sequential *t*-test analysis of regime shifts (STARs) (Rodionov, 2004; Rodionov and Overland, 2005;

Howard et al., 2007; www.BeringClimate.noaa.gov). The STARs use a *t*-test analysis to determine whether sequential records in a time series represent statistically significant departures from mean values observed during the preceding period of a predetermined duration. The cutoff length (*l*) is set to 30 years, and the probability level to $\alpha = 0.1$.

The Adjacent-Averaging filter smooth was used to remove noise from signals by OriginPro8.0 software; for example, the measured $\delta^{15}N$ and marine OC have smoothed 5 points of window. Geochemical data were interpolated to obtain evenly spaced time series using OriginPro8.0 software prior to statistical analyses. The rule of interpolation is according to the resolution of data; as the result of the different resolutions of this study to others, all records are interpolated to annual resolution. When all of the data were adjusted to the same resolution, IBM SPSS Statistics software was further used for correlation analysis.

3 Results

3.1 Chronology of the core

The chronology of core SBB-190629 was determined by ^{210}Pb dating through a gamma spectrometer. In the ^{238}U – ^{206}Pb decay series, ^{226}Ra ($T_{1/2} = 1,600$ years), ^{214}Pb ($T_{1/2} = 26.8$ min), and ^{214}Bi ($T_{1/2} = 19.9$ min) are the parents of ^{210}Pb ($T_{1/2} = 22.3$ years). If sample material is formed more than 200 years ago, its ^{226}Ra and ^{210}Pb activities reach secular equilibrium (i.e., the activities

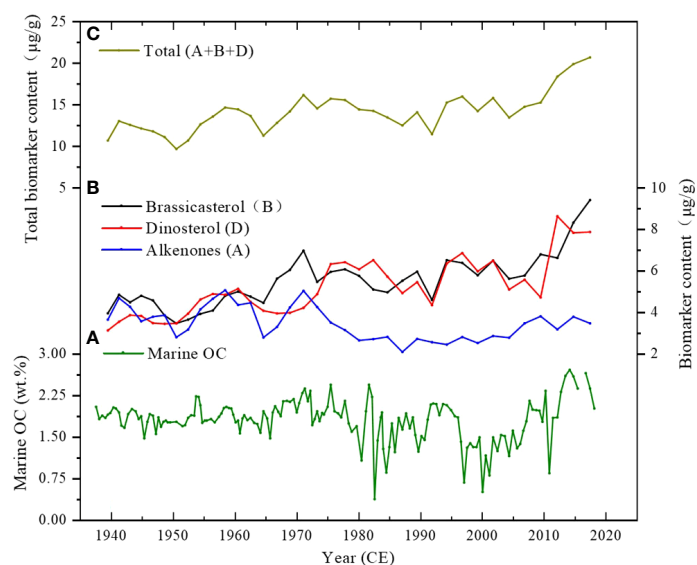


FIGURE 4

(A) Variation of marine organic carbon (OC) calculated by C/N atom ratio in core SBB-190629. Content of marine biomarkers was expressed in μg per g dry sediment ($\mu\text{g/g}$). (B) Total marine biomarkers calculated by A + B + D. (C) Variation of individual marine biomarkers: Brassicasterol (B), Dinosterol (D), and Alkenones (A).

are equal). Similarly, after the sample formation is more than 1 day, its ^{214}Pb , ^{214}Bi , and ^{210}Pb reach secular equilibrium. Therefore, we can use ^{226}Ra , ^{214}Pb , and ^{214}Bi to obtain the supported ^{210}Pb . Excess ^{210}Pb comes from ^{222}Rn ($T_{1/2} = 3.8$ days) decay in the atmosphere and precipitates on Earth through wet and dry fallouts. As excess ^{210}Pb deposits on the Earth's surface, its decay timer starts to count. Therefore, excess ^{210}Pb in a sediment sequence exponentially decreases with time (or depth) (Li et al., 2019):

$$^{210}\text{Pb} = ^{210}\text{Pb}_0 \times e^{-\lambda t} = ^{210}\text{Pb}_0 \times e^{-\lambda D/SR} \quad (2)$$

where D and SR represent depth and sedimentation rate, respectively. The slope of the $\ln ^{210}\text{Pb}$ -D plot should yield a linear sedimentation rate (SR) (Appleby and Oldfield, 1992). Figure 2C shows the excess ^{210}Pb decay trend with the core depth. Because the excess ^{210}Pb activity is much higher than the supported ^{210}Pb activity, the decay trends of excess ^{210}Pb and total ^{210}Pb are very similar. With the use of ^{226}Ra or $(^{214}\text{Pb} + ^{214}\text{Bi})/2$ as supported ^{210}Pb for calculation of excess ^{210}Pb , the fitting results are similar. Considering ^{214}Pb and ^{214}Bi can quickly reach secular equilibrium with ^{210}Pb , we choose to use the excess ^{210}Pb calculated from the total ^{210}Pb minus $(^{214}\text{Pb} + ^{214}\text{Bi})/2$. An equation of $y = 1226.8 \times e^{-0.055116x}$ is obtained by using exponential fitting of the excess ^{210}Pb with depth. The estimated SR in SBB-190629 is 0.564 cm/year (Figure 2C). Based on this SR, the 46-cm-long core would cover about 80 years of depositional history. With the use of the SR of 0.564 cm/year, the age of each depth can be calculated assuming the age of the top sediment was 2019 CE.

3.2 $\delta^{15}\text{N}$, total organic carbon, and total nitrogen variation of core SBB-190629

The $\delta^{15}\text{N}_{\text{sed}}$ in core SBB-190629 varies from 6.24‰ to 7.43‰ (Figure 3A). The variation of $\delta^{15}\text{N}_{\text{sed}}$ fluctuated between 6.70‰ and 7.20‰ from the late 1930s to the 1960s and then became higher during the 1970s with an average of 7.14‰. After that, a decline in $\delta^{15}\text{N}_{\text{sed}}$ of ~1‰ was evident from the mid-1980s to the mid-2000s. After that, the $\delta^{15}\text{N}_{\text{sed}}$ value increased sharply in the mid-2000s and reached 7.30‰ in 2015–2016.

The TOC of the samples varies from 3.37 to 6.19 wt.% (Figure 3B, blue). A decrease to approximately 2 wt.% occurred between the late-1930s and mid-1980s. The TOC further decreased with an average of 4.28 wt.% between the mid-1980s and mid-2000s. A sharp increase in TOC with a maximum at 6.19 wt.% was evident since the mid-2000s.

Sedimentary TN consists of organic nitrogen (ON) and inorganic nitrogen (IN). The TN of sediments in core SBB-190629 fluctuates between 0.38 and 0.64 wt.% (Figure 3B, green). The variation trend of TN is similar to that of TOC.

According to the results of STARS analysis, the regime shifts of TOC, TN, and $\delta^{15}\text{N}$ approximately appear at the same time: 1965~1970, 1978~1985, and 2005~2010 (Figure S1). In general, the variation of TOC, TN, and $\delta^{15}\text{N}$ roughly displayed similar temporal trends.

3.3 Marine organic carbon calculated by C/N and marine biomarkers

The C/N ratios (atom ratio of TOC/TN) in core SBB-190629 vary from 9.73 to 12.61, with an average of 10.53 (Figure 3C). Although both marine and terrigenous origins of organic matters could contribute to the sediments in the coring site, the good correlation between TOC and TN (Figure 3) suggests that the majority of the organic matters in the sediments came from the similar source. For the linear equation of $\text{TN} = 0.092 * \text{TOC} + 0.081$ ($R^2 = 0.81$, $p < 0.01$) (Figure S2), the intercept represents the average 0.081 wt.% of IN in the TN, which may be from terrestrial clay-bound N (Müller, 1977; Schubert and Calvert, 2001; Hu et al., 2013; Hendy et al., 2015; Wang et al., 2019). Compared to the average TN of 0.48 wt.% in SBB sediments, the IN accounts for about 16.9% of TN, so its interference is minor.

The C/N ratio has been utilized for assessing the source of organic matter. Generally, the C/N ratio of algae ranges from 4 to 10 (Thornton and McManus, 1994; Lamb et al., 2006), while the C/N ratio of approximately 20 indicates terrestrial vascular plant input (Meyers, 1997; Schubert and Calvert, 2001). A two-end-member mixing model was employed to estimate the relative contributions of OC from marine and river in the SBB sediments.

$$(C/N)_{\text{sample}} = f_{\text{terrestrial}} \times (C/N)_{\text{terrestrial}} + f_{\text{marine}} \times (C/N)_{\text{marine}} \quad (3)$$

$$f_{\text{terrestrial}} + f_{\text{marine}} = 1 \quad (4)$$

The terrestrial end-member is based on the mean values of the particular matter samples collected near Santa Clara River ($C/N_{\text{terrestrial}} = 13.07$), which is the main terrestrial source of the SBB sediments (Masiello and Druffel, 2001; Komada et al., 2004). The average C/N ratio of phytoplankton is 7 for the marine end-member (Lamb et al., 2006). The $\text{OC}_{\text{marine}}$ is calculated by multiplying the sediment proportion of marine by TOC; the trends are shown in Figure 4A. According to this calculation, the average values of $\text{OC}_{\text{marine}}$ content and f_{marine} are 1.83 wt.% (ranging from 0.39 to 2.76 wt.%) and 41% (ranging from 12% to 55%), respectively. Compared with the average TOC content of 4.31 wt.%, the $\text{OC}_{\text{marine}}$ proportion in the TOC is generally less than the $\text{OC}_{\text{terrestrial}}$, agreeing with the previous studies (Thunell, 1998; Hendy et al., 2015).

Brassicasterol (B) and Dinosterol (D) are major marine sediment biomarkers in SBB derived predominantly from cell membrane components of diatom and dinoflagellate among phytoplankton, which further reflect the corresponding

phytoplankton biomass in the euphotic layer (Volkman, 1986; Volkman et al., 1998; Xing et al., 2016). Alkenones (A) are another major lipid component that originated from haptophytes. Hence, the sum of Brassicasterol, Dinosterol, and Alkenones (B + D + A) can be successfully utilized for evaluating primary productivity (Schubert et al., 1998; Xing et al., 2016). The biomarker contents of the three lipid biomarkers are depicted in Figure 4B. Brassicasterol and Dinosterol contents gradually increased before the 1970s, slightly decreased after the 1980s, and increased again from the 2000s, consistent with TOC and OC_{marine} variations. Alkenone content decreased gradually over the last 80 years, despite a slightly high value in the late 1950s and early 1970s. The sum of the three biomarkers shows decadal variations and a strongly increasing trend from 2010 onward (Figure 4C).

4 Discussions

4.1 The influence of $\delta^{15}\text{N}$ signals transported from the eastern tropical North Pacific on Santa Barbara Basin

As mentioned above, surface water inputs to SBB have different $\delta^{15}\text{N}$ with heavier $\delta^{15}\text{N}$ of CUC originating from ETNP and lighter $\delta^{15}\text{N}$ of CC. In order to provide evidence of high $\delta^{15}\text{N}$ waters from ETNP that could be advected to Southern California *via* CUC to influence the water $\delta^{15}\text{N}$ along the Southern California Coast, we collected integrated $\delta^{15}\text{N}$ of nitrate (Sigman et al., 2003; Sigman et al., 2005) and salinity data sets of water samples within 100–400 m from the California Coast to the southern tip of Baja California (Van Geen, 2001). Figure S3 shows a strong positive correlation ($R^2 = 0.97$) between $\delta^{15}\text{N}$ and salinity, and the highest $\delta^{15}\text{N}$ and salinity in the southern tip of Baja California decreased to the lowest $\delta^{15}\text{N}$ and salinity near SBB. The conservative behavior of $\delta^{15}\text{N}$ with respect to salinity demonstrates the ETNP influence on the water along the California Coast. Although the CUC is the strongest in fall, Liu and Kaplan (1989) found a similar correlation between $\delta^{15}\text{N}$ and salinity along the California Coast water in the summer. In addition, as already noted, $\delta^{15}\text{N}_{\text{sed}}$ from the SBB records the variation of $\delta^{15}\text{N}$ in the water column; therefore, a positive correlation between $\delta^{15}\text{N}$ from an SBB box core (SPR0901-04BC, Figure 1A) and measured salinity at the core of CUC ($\sigma\theta = 26.4\text{--}26.5$) from the CalCOFI during the last 50 years was verified by Wang et al. (2019) to support the influence of ETNP high $\delta^{15}\text{N}$ on SBB. Thus, ETNP water is an important source of enriched $\delta^{15}\text{N}_{\text{nitrate}}$ transported to SBB with the CUC.

Another test to demonstrate the ETNP $\delta^{15}\text{N}$ influence on the $\delta^{15}\text{N}$ signal in SBB is to use $\delta^{15}\text{N}_{\text{sed}}$ in ETNP to compare with the SBB $\delta^{15}\text{N}_{\text{sed}}$. The $\delta^{15}\text{N}_{\text{sed}}$ record of core SBB-190629 is compared with the $\delta^{15}\text{N}_{\text{sed}}$ records at three sites along the North

American margin (Figure 5). The Pescadero Slope and Soledad Basin sites (Figure 1B) are within the anoxic zone in the ETNP (Deutsch et al., 2014). Adjacent to SBB, the third site in Santa Monica Basin (SMB, Figure 1B) is >1,000 km north of the anoxic zone but physically connected *via* the coastal undercurrent (Deutsch et al., 2014). Basically, the $\delta^{15}\text{N}_{\text{sed}}$ records at the Pescadero Slope and Soledad Basin sites reflect the strongest influence of the ETNP $\delta^{15}\text{N}$ (or the distal $\delta^{15}\text{N}$ signal), whereas the SBB and SMB sites are farther away from the ETNP influence. Despite the four cores having their own chronologies, the comparisons shown in Figure 5 reveal that 1) $\delta^{15}\text{N}_{\text{sed}}$ records (except the SBB $\delta^{15}\text{N}_{\text{sed}}$) showed a general decreasing trend from the late 1930s to ~1980. All four records showed relatively low values during 1980–2000 and then increasing trends after 2000. 2) The $\delta^{15}\text{N}_{\text{sed}}$ values became lower from the south site to the north site, indicating that the mixture from the ETNP $\delta^{15}\text{N}$ becomes weaker with increasing distance from ETNP. The latitudinal and chronological comparisons of the $\delta^{15}\text{N}_{\text{sed}}$ records at the four sites along the Eastern Pacific margin exhibit that the $\delta^{15}\text{N}_{\text{sed}}$ have recorded primarily large-scale oceanographic changes originating in the water column, and the water with the ETNP $\delta^{15}\text{N}$ signal can reach as far as the SBB, implying that the distal $\delta^{15}\text{N}$ signal should be distinguished from the local $\delta^{15}\text{N}$ signal in the SBB $\delta^{15}\text{N}_{\text{sed}}$. The visible dissimilarities on short timescales between the SBB $\delta^{15}\text{N}_{\text{sed}}$ record and other $\delta^{15}\text{N}_{\text{sed}}$ records further validate the local $\delta^{15}\text{N}$ signal interference. Below, we discuss the determination of the local $\delta^{15}\text{N}$ signal in the SBB $\delta^{15}\text{N}_{\text{sed}}$.

4.2 Estimation of the local $\delta^{15}\text{N}$ signal in Santa Barbara Basin

To distinguish the local $\delta^{15}\text{N}$ signal in SBB, the $\delta^{15}\text{N}_{\text{sed}}$ of Pescadero Slope and Soledad Basin belonging to the anoxic zone of ETNP were treated to represent the ETNP $\delta^{15}\text{N}$ variability (Deutsch et al., 2014). These two records from 1935 to 2010 were selected to keep the same timescale for this study. The $\delta^{15}\text{N}$ anomalies ($\Delta\delta^{15}\text{N}$) of ETNP were calculated by the individual $\delta^{15}\text{N}_{\text{sed}}$ value by subtracting the mean $\delta^{15}\text{N}$ value over 1935–2007 of each site and then averaging them. Figure 6A shows the ETNP $\Delta\delta^{15}\text{N}$ record (blue curve with shaded error area) during 1935–2007. In order to confirm the representative of the ETNP $\delta^{15}\text{N}$ signal, we compared the simulated changes in $\delta^{15}\text{N}$ (Figure 6A, green curve) using an ocean general circulation model (GCM) by Deutsch (2014) with our result. The modeled $\delta^{15}\text{N}$ record was based on numerical simulations of the cycle of N and its isotope cycle in the ETNP anoxic zone (125°W to coast, 5°N to 25°N) during 1959–2005. The result shows that decadal variations in the model predicted $\delta^{15}\text{N}$ of particulate organic N sinking into the anoxic zone, which closely matches the sediment proxy data in both amplitude and timing. The reliability of the calculated ETNP $\delta^{15}\text{N}$ signal is verified.

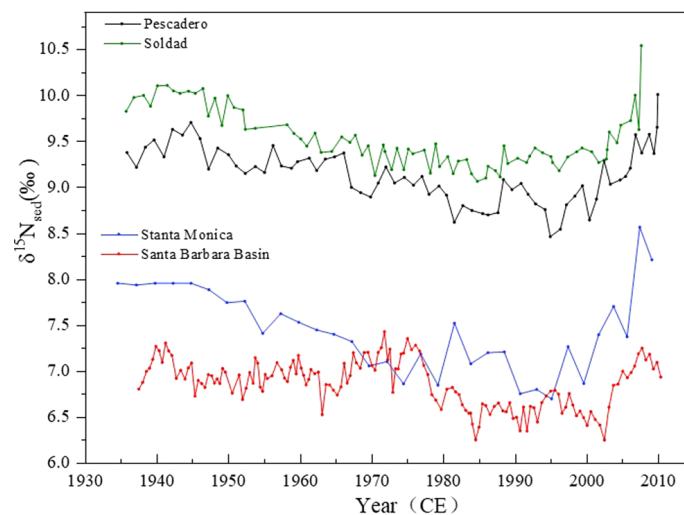


FIGURE 5

Bulk organic $\delta^{15}\text{N}$ from four sediment core sites along the North American margin: Soledad (Deutsch et al., 2014), Pescadero (Deutsch et al., 2014), Santa Monica Basin (Davis et al., 2019), and Santa Barbara Basin (this study). Locations of core sites are showing in Figure 1B.

Similarly, the $\Delta\delta^{15}\text{N}$ ($\delta^{15}\text{N}$ anomaly, deviation from the mean $\delta^{15}\text{N}$ of 1935~2007) record for the SBB $\delta^{15}\text{N}_{\text{sed}}$ record was obtained. By subtracting the ETNP $\Delta\delta^{15}\text{N}$ from the SBB $\Delta\delta^{15}\text{N}$, the local $\Delta\delta^{15}\text{N}$ in SBB ($\Delta\delta^{15}\text{N}_{\text{SBB}}$) was produced, shown in Figure 6B (red curve). Note that the local anomaly signals are only accessible from 1938 to 2007 owing to the lack of availability of the ETNP $\Delta\delta^{15}\text{N}$ since 2007. In Figure 6B, the $\Delta\delta^{15}\text{N}_{\text{SBB}}$ record ranges from -0.5 to 0.6 , and the difference between the maximum and minimum value is 1.1 , roughly equal to the change of bulk $\Delta\delta^{15}\text{N}$ (1.2); therefore, the local effect of $\delta^{15}\text{N}_{\text{sed}}$ is not insignificant. In addition, there are differences in the trend of $\Delta\delta^{15}\text{N}_{\text{SBB}}$ and bulk $\Delta\delta^{15}\text{N}$; the $\Delta\delta^{15}\text{N}_{\text{SBB}}$ appeared in decadal variations with a general increasing trend from 1945 to the late 1970s and a decreasing trend afterward. The outstanding peak of the $\Delta\delta^{15}\text{N}_{\text{SBB}}$ is during 1965~1978. In the following sections, we will discuss the causes of the variations in the $\Delta\delta^{15}\text{N}_{\text{SBB}}$.

4.3 Forcing factors on local $\Delta\delta^{15}\text{N}$ signal variation in Santa Barbara Basin on interannual timescales

4.3.1 Changes in the strength of bottom water denitrification in Santa Barbara Basin

The main influencing factors for the $\Delta\delta^{15}\text{N}_{\text{SBB}}$ fluctuations are i) incomplete nitrate utilization, ii) terrestrial input, and iii) bottom water denitrification. First of all, in Section 3.3, we have demonstrated that the IN accounted for 16.9% of the TN on average in the sediments. This IN mainly from terrestrial

clay-bound N (Hendy et al., 2015; Wang et al., 2019) has little influence on the SBB $\delta^{15}\text{N}_{\text{sed}}$. How the influence of terrestrial input of organic N is compared with TN from the water column in SBB remains unclear. Secondly, the additionally isotopic variability arising from incomplete surface nutrient utilization is insignificant in magnitude and also confined to seasonal timescales (Emmer and Thunell, 2000; Davis et al., 2019). Therefore, Factors i) and ii) may have minor impacts on the $\Delta\delta^{15}\text{N}_{\text{SBB}}$ fluctuations on interannual timescales. In this present work, bottom water denitrification is thought to majorly impact local $\delta^{15}\text{N}$ variability. Denitrification in the anoxic waters and sediments in a semi-closed environment of SBB has been well documented in historic and modern records (Emmer and Thunell, 2000; Bograd et al., 2002; Goericke et al., 2015; Davis et al., 2019). SBB is influenced by Southern California eddy, which through strong vertical advection enhances water mixing (Chenillat et al., 2018). Chung (1973) reported a ^{222}Rn -based estimate of $3.9 \text{ cm}^2/\text{s}$ for vertical eddy diffusivity in SBB, which yields a rough mixing time of 0.6–0.8 years for the basin water, implying significant and rapid water exchange across the bottom water and the overlying water (Sigman et al., 2003). In addition, tight correlations were observed between our $\Delta\delta^{15}\text{N}_{\text{SBB}}$ record and local redox proxies (Re/Mo ratio and C_{29} stanol/stenol ratio), which document SBB bottom water O_2 condition (see the detailed discussion as follows), providing evidence that SBB local denitrification process affects sediment $\delta^{15}\text{N}$ signal.

Molybdenum (Mo) and rhenium (Re) are redox-sensitive elements and can be accumulated in marine sediments beneath O_2 -depleted waters. However, authigenic Mo precipitation

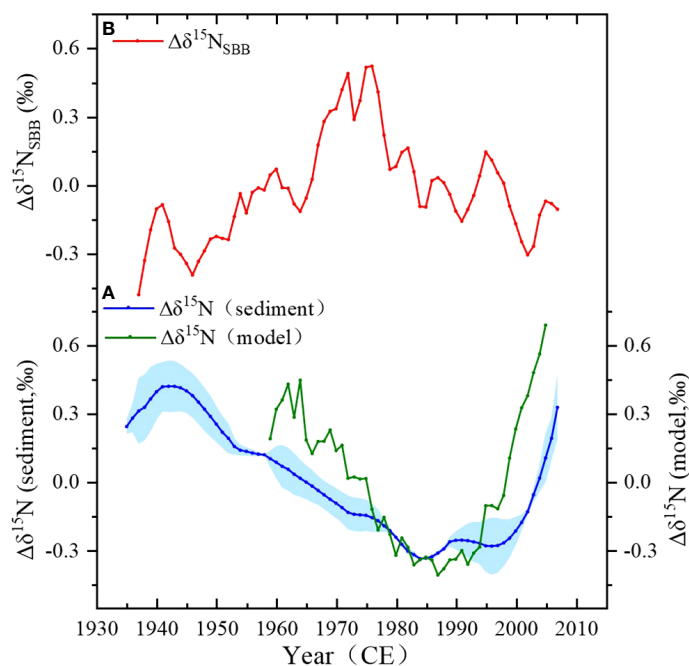


FIGURE 6
 Calculation of ETNP $\Delta\delta^{15}\text{N}$ and $\Delta\delta^{15}\text{N}_{\text{SBB}}$. **(A)** Construction of the eastern tropical North Pacific (ETNP) $\Delta\delta^{15}\text{N}$ signal, the blue curve shows the result of the average $\Delta\delta^{15}\text{N}$ from Soledad and Pescadero sites, and the green curve shows the result of the model. **(B)** The calculated $\Delta\delta^{15}\text{N}_{\text{SBB}}$ (red curve).

only proceeds in the presence of free HS^- water, which is considered a more reducing environment compared with authigenic Re precipitation (Crusius et al., 1996). Thus, a decrease in sedimentary Re/Mo indicates the pore water shift from slightly to strongly reducing sulfidic environments (Crusius et al., 1996; Wang et al., 2017). In anoxic marine environments such as SBB, Re/Mo ratio in marine sediments is used to indicate changing redox conditions at the time of sediment deposition, with a higher Re/Mo ratio reflecting lower redox potential, or enhanced ODZ and denitrification degree and vice versa (Wang et al., 2017). Wang et al. (2017) measured total Mo and Re concentrations in the sediments and calculated enrichment factors for Re/Mo $\{(Re/Mo)_{\text{EF}}; 3\text{-year resolution}\}$ in SBB from 1759 to 2008. In order to compare with this record, a linear extrapolation was used to obtain annual resolution by using Origin software. The $\Delta\delta^{15}\text{N}_{\text{SBB}}$ record of core SBB-190629 was compared with the $(Re/Mo)_{\text{EF}}$ record (Figure 7B) of core SPR0901-04BC, showing a strong negative correlation ($r = -0.49, p < 0.05$) which demonstrates that the $\Delta\delta^{15}\text{N}_{\text{SBB}}$ was controlled by redox conditions.

Another redox-sensitive proxy in SBB is the C_{29} stanol/stenol ratio, as the $5\alpha(\text{H})\text{-stanol}/\Delta 5\text{-stanol}$ ratios increase through microbial conversion under anoxic conditions by the reduction of sterol $\Delta 5$ double bonds to $5\alpha(\text{H})\text{-stanols}$ (Rosenfeld and Hellmann, 1971; Eyssen et al., 1973). Thus, the C_{29} stanol/

stenol ratio is used as an indicator of redox conditions related to oxygen availability in the sediments and bottom waters of the SBB, with a higher C_{29} stanol/stenol ratio reflecting lower redox potential, stronger anoxia, and denitrification and vice versa (Alfken et al., 2020). Alfken et al. (2021) used a matrix-assisted laser desorption/ionization coupled to Fourier transform-ion cyclotron resonance-mass spectrometry (MALDI-FT-ICR-MS) to measure C_{29} stanol/stenol from 1900 to 2009 (Figure 7C). We take the part of 1935–2009 for the comparison. In Figure 7, a general positive correlation between the C_{29} stanol/stenol ratio and $\Delta\delta^{15}\text{N}_{\text{SBB}}$ records further suggests that the change of $\Delta\delta^{15}\text{N}_{\text{SBB}}$ represents SBB bottom water denitrification. Note that the C_{29} stanol/stenol record was a few years ahead of the $\Delta\delta^{15}\text{N}_{\text{SBB}}$ record, which might be caused by chronological uncertainties or other unknown reasons. After the C_{29} stanol/stenol record was moved 5 years later, the positive correlation between the two records reaches the highest ($r = 0.61, p < 0.01$).

In summary, Figure 7 illustrates that the variations of the $\Delta\delta^{15}\text{N}_{\text{SBB}}$ record reflect changes in bottom water denitrification in SBB, with an increased $\Delta\delta^{15}\text{N}_{\text{SBB}}$ indicating reduced oxygen content and enhanced denitrification. According to the $\Delta\delta^{15}\text{N}_{\text{SBB}}$ record, the bottom water denitrification increased generally from 1945 to the late 1970s and then decreased at around 2000. The mechanisms controlling denitrification in SBB are discussed in detail as follows.

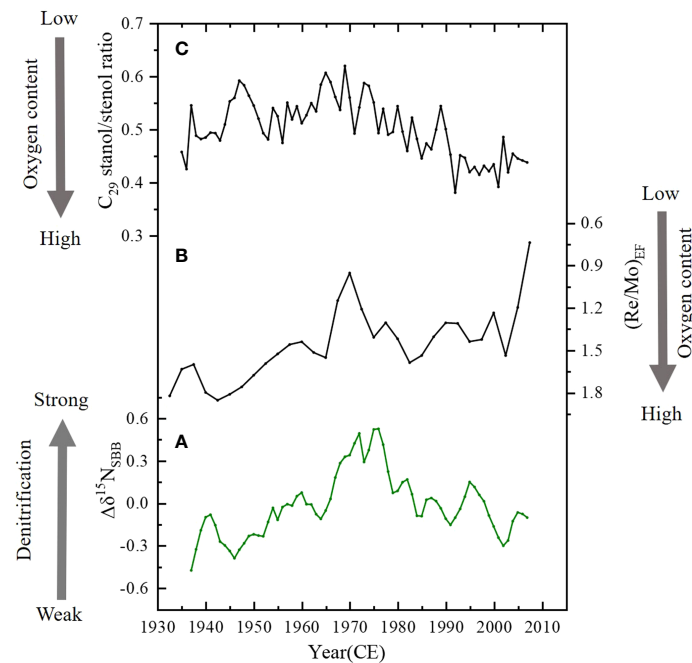


FIGURE 7

Comparisons of the (A) $\Delta\delta^{15}\text{N}_{\text{SBB}}$ with redox proxies: (B) $(\text{Re}/\text{Mo})_{\text{EF}}$ record (Wang et al., 2017) and (C) C_{29} stanol/stenol ratio record (Alfken et al., 2021). Note that the scale of $(\text{Re}/\text{Mo})_{\text{EF}}$ record is reversed.

4.3.2 The effect of upwelling and marine productivity on the variation of Santa Barbara Basin local $\delta^{15}\text{N}$ signal

As mentioned earlier, denitrification in SBB bottom water can be affected by 1) oxygen consumption of OC, which is related to marine productivity, and 2) O_2 input by flushing water from north of Point Conception, which are tightly connected with the local upwelling process. Variability of the upwelling north of Point Conception has been monitored since 1946 and can be described by the Pacific Fisheries Upwelling Index (PFEL) at 36°N (Davis et al., 2019). Upwelling provides nutrients to support phytoplankton growth in SBB (Checkley and Barth, 2009); stronger upwelling will cause higher productivity and result in higher marine OC (Wang et al., 2019). The general trend of marine OC (Figure 4) shows significant variability on a decadal timescale. The averages and standard deviations during 1937~1966, 1966~1982, 1982~2007, and 2007~2010 were 1.87 ± 0.16 ($n = 61$), 2.03 ± 0.27 ($n = 23$), 1.53 ± 0.42 ($n = 47$), and 2.10 ± 0.50 ($n = 19$) wt.%, respectively. The average and standard deviation during 1937~1966 indicate that the $\text{OC}_{\text{marine}}$ had a small variation and was close to the average (1.83 wt.%) of the entire record. High contents prevailed during 1966~1982, and low $\text{OC}_{\text{marine}}$ contents occurred during 1982~2007. However, the $\text{OC}_{\text{marine}}$ record may involve a diagenetic effect. Marine biomarkers are considered an effective proxy for their resistance to sedimentary diagenesis and stable preservation in geological

time, thus providing an independent measure of export productivity in the SBB water column. Figure 8 compares the $\Delta\delta^{15}\text{N}_{\text{SBB}}$ record (Figure 8A), the $\text{OC}_{\text{marine}}$ record (Figure 8B), total marine biomarker (B + D + A) record (Figure 8C), and annual average upwelling index (Figure 8D). The comparisons showed good correlations among the four curves, indicating that higher $\text{OC}_{\text{marine}}$ and total marine biomarker contents that resulted from higher productivity under stronger upwelling caused stronger denitrification in the SBB bottom water. According to the positive relationship between the $\Delta\delta^{15}\text{N}_{\text{SBB}}$ record and primary productivity records ($\Delta\delta^{15}\text{N}_{\text{SBB}}$ and $\text{OC}_{\text{marine}}$: $r = 0.40$, $p < 0.01$; $\Delta\delta^{15}\text{N}_{\text{SBB}}$ and marine biomarkers: $r = 0.61$, $p < 0.01$), enhanced productivity caused by upwelling (upwelling index and marine biomarkers $r = 0.63$, $p < 0.01$) should be more important than the O_2 brought by flushing events from north of Point Conception to the denitrification in the bottom water of the SBB. This probably means that 1) the O_2 amount brought by flushing events may be small, 2) the duration of the flushing events is short, and 3) the low O_2 but high nutrient upwelled water is dominant so that the annual hypoxia condition of SBB would not be affected significantly by the flushing O_2 amount. Therefore, upwelling and productivity seem to be the major factors to influence the $\delta^{15}\text{N}$ in SBB.

Several studies have also found that local upwelling-induced productivity may cause the sediment $\delta^{15}\text{N}$ changes in SBB,

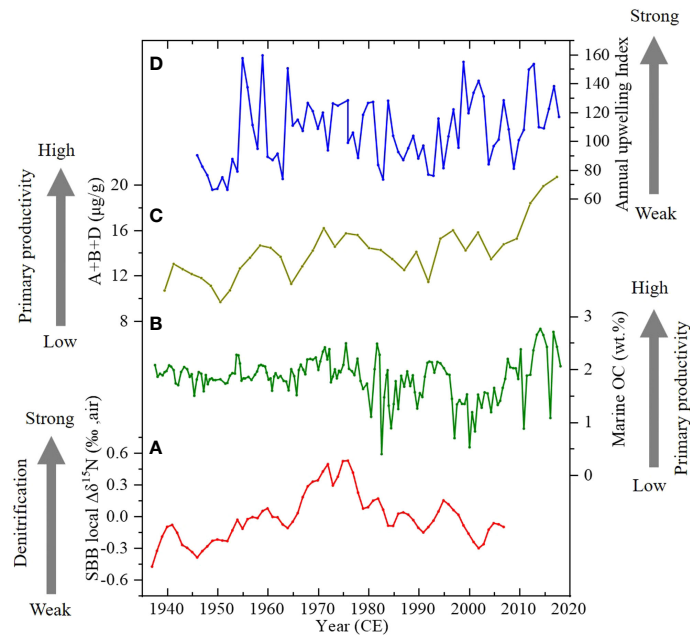


FIGURE 8 Comparisons of (A) the $\Delta\delta^{15}N_{SBB}$, (B) OC_{marine} (wt.%), and (C) total biomarker content in core SBB-190629 with (D) annual average upwelling index in $36^{\circ}N$ at the north of Point Conception (Davis et al., 2019).

supporting our finding above (Wang et al., 2019; Sánchez et al., 2022). Wang et al. (2019) also proposed that nutrient-rich, higher $\delta^{15}N$ subarctic water, which was caused by incomplete nitrate utilization in the subarctic region when the Aleutian low is strong, might have been transported into the SBB and was recorded by sediment $\delta^{15}N$ during the Little Ice Age period. Indeed, a high-value state was found between 1965 and 1980 in our SBB $\delta^{15}N_{sed}$ when PDO was in the negative phase. Considering the phase relationship of negative PDO vs weak Aleutian Low (Chavez et al., 2003; Hendy et al., 2015), the southward transport mechanism could not explain the high SBB $\delta^{15}N_{sed}$ signal during 1965~1980, whereas the marine biomarkers, marine OC, and local redox proxies all support higher productivity and strengthened local denitrification in SBB during this time interval. Therefore, we suggest that the high value between 1965 and 1980 is more likely to be the result of local denitrification.

4.4 Local and remote forcing on $\delta^{15}N$ variations in Santa Barbara Basin

There have been many studies focusing on the climate effect on the bulk SBB $\delta^{15}N_{sed}$ (Emmer and Thunell, 2000; Tems et al., 2015; Horak et al., 2016; Davis et al., 2019; Wang et al., 2019); however, studies specifically about the separate signals are

limited. Since the variability of upwelling strength in the California Coast system on annual-to-decadal timescales is linked with ENSO (e.g., Bograd and Lynn, 2001), PDO (e.g., Chhak and Di Lorenzo, 2007), and NPGO (e.g., Di Lorenzo et al., 2008; García-Reyes and Largier, 2010), here we discuss the influences of the climatic forcing on the upwelling, production, and denitrification in SBB. In Figure 9, the records of ENSO, PDO, and NPGO were compared with the records of upwelling, marine biomarkers, OC_{marine} (reflecting marine productivity), and the $\Delta\delta^{15}N_{SBB}$.

4.4.1 The role of tropical trade winds on $\delta^{15}N_{sed}$ signature as a remote influencing factor

The ETNP denitrification is controlled by the variations in wind intensity over the tropical Pacific by eventually regulating the ocean water upwelling, the zonal structure of the underlying thermocline, area of oxygen minimum zone (OMZ), and biological productivity (Canfield, 2006; Deutsch et al., 2014; Tems et al., 2015; Horak et al., 2016). Stronger tropical trade winds will generate stronger upwelling along the equator divergent zones and enhance primary productivity (Sydeman et al., 2014). Consequently, the area of OMZ and denitrification in ETNP will be intensified, thus elevating $\Delta\delta^{15}N$ of ETNP (Deutsch et al., 2014). The variations of $\delta^{15}N$ signals by ETNP denitrification are further transported northward by CUC and

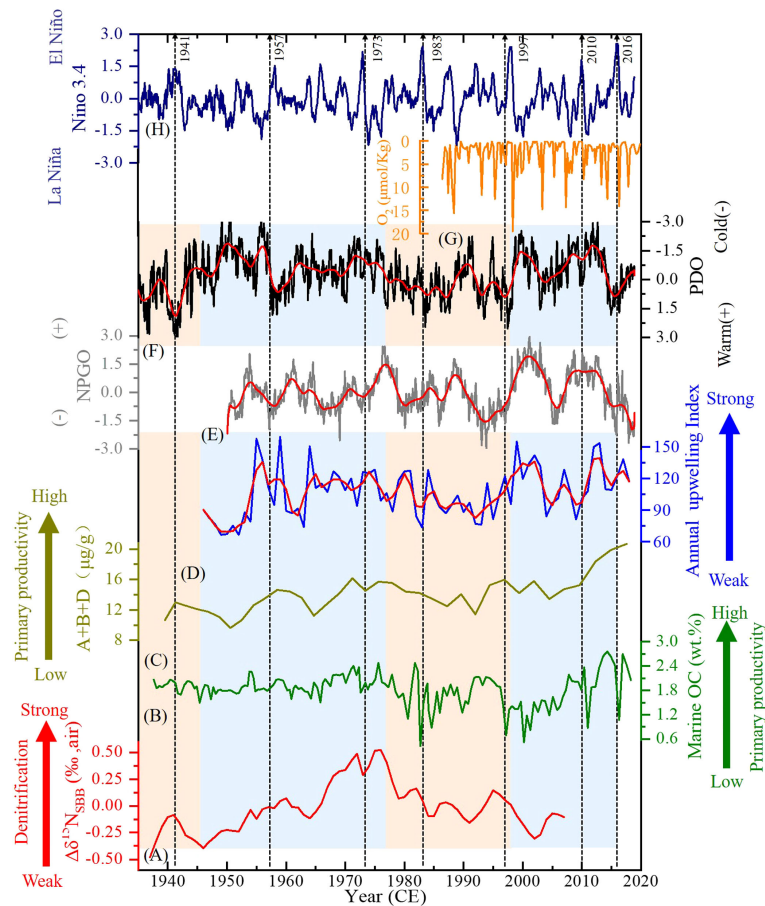


FIGURE 9
 Comparisons of the Santa Barbara Basin (SBB) (A) local $\Delta\delta^{15}\text{N}$ (‰), (B) $\text{OC}_{\text{marine}}$ (wt.%), (C) marine biomarkers ($\mu\text{g/g}$), (D) annual upwelling index, and (G) O_2 content ($\mu\text{mol/kg}$) records with (E) North Pacific Gyre Oscillation (NPGO) (<http://www.o3d.org/ngpo/>), (F) Pacific Decadal Oscillation (PDO) (<http://jisao.washington.edu/pdo/PDO>), and (H) El Niño–Southern Oscillation (ENSO) (https://www.esrl.noaa.gov/psd/gcos_wgsp/Timeseries/) records. Strong El Niño events such as in 1941, 1957–1958, 1973, 1982–1983, 1997–1998, 2010, and 2016 are marked. Red lines in panels (D–F) represent the results of 3 years smoothed. Orange areas denote warm phase of PDO, whereas blue areas represent cold phase of PDO. Note that the scale of O_2 content and PDO is reversed.

finally recorded in SBB water and sediments. Therefore, tropical trade winds act as a remote influencing factor and control the general trend of SBB sedimentary $\delta^{15}\text{N}$ ($\delta^{15}\text{N}_{\text{sed}}$) signature. The general decreasing trends of the $\delta^{15}\text{N}_{\text{sed}}$ records shown in Figure 5 from 1940 to the late 1980s (except the SBB record) reflect reduced upwelling, productivity, and denitrification in the ETNP probably caused by the weakening of tropical trade wind (Deutsch et al., 2014; Tems et al., 2015). The strength of tropical trade wind remained low during 1980–2000 and then started to increase. Except for high values between 1965 and 1980, the SBB $\delta^{15}\text{N}_{\text{sed}}$ variation follows that of the ETNP, suggesting that tropical trade wind induced ETNP water column $\delta^{15}\text{N}$ change, which controlled the general trend of SBB $\delta^{15}\text{N}_{\text{sed}}$. After the removal of the distal $\delta^{15}\text{N}$ signature (the ETNP $\delta^{15}\text{N}$) from the SBB $\delta^{15}\text{N}_{\text{sed}}$ record, the local mechanism of the $\Delta\delta^{15}\text{N}_{\text{SBB}}$ trend needs an explanation.

4.4.2 The role of El Niño–Southern Oscillation, Pacific Decadal Oscillation, and North Pacific Gyre Oscillation on $\delta^{15}\text{N}_{\text{sed}}$ signature as a local controlling factor

The PDO is a long-term ocean fluctuation at the mid-latitudes of the Pacific Ocean and is controlled by the ocean–atmosphere climatic variability (Deser et al., 2004; Di Lorenzo et al., 2008). It is determined by the first dominant mode of variations in sea surface temperature (SST) and has triggered major environmental alterations in terms of physical and biological regime shifts along the western coast of North America (Di Lorenzo et al., 2008). The PDO shifts reflect changes in the strength and position of Aleutian low and concomitant changes in upwelling and SST, which have major environmental impacts in the area of SBB (Hendy et al., 2015). As shown in Figure 9, the positive (warm) PDO phase is

associated with depressed thermocline and weakened upwelling with shallow water depth and therefore induces a significant decline in marine productivity in SBB (Chavez et al., 2003; Venrick, 2012; Hendy et al., 2015; Wang et al., 2017). The decreased marine productivity of positive PDO reduces bottom water denitrification, further inducing a decline of $\Delta\delta^{15}\text{N}_{\text{SBB}}$. In contrast, the negative (cold) PDO phase is associated with higher productivity in SBB, which is attributed to intensified ocean water upwelling induced by the Aleutian low (Chavez et al., 2003; Di Lorenzo et al., 2008; Hendy et al., 2015), therefore increasing the $\Delta\delta^{15}\text{N}_{\text{SBB}}$ by enhancing bottom water denitrification in SBB. Hence, the PDO regime shift has a determining influence on the general trend of $\Delta\delta^{15}\text{N}_{\text{SBB}}$ on the decadal to centennial timescale.

The NPGO is a climate pattern that emerges as the second dominant mode of sea surface temperature variability in the Northeast Pacific and is driven by the atmosphere through the North Pacific Oscillation (Ceballos et al., 2009). The wind-driven upwelling and horizontal advection are the main driving factors of NPGO fluctuations, and their variations are correlated with salinity, nutrients, and chlorophyll of the central and eastern branches of the subtropical gyre (Di Lorenzo et al., 2008). However, the NPGO impact cannot be addressed before 1950 owing to the availability of NPGO indices only after 1950. According to the observation, positive correlations between the salinity, NO_3^- content, and Chl-*a* of CC and NPGO strength (Di Lorenzo et al., 2008) imply that stronger NPGO causes stronger upwelling in the south of 38°N areas. However, only a weak positive correlation between NPGO and upwelling ($r = 0.27$, $p < 0.05$) in SBB may be due to the alternating effects of the phase relationship between fluctuations of the PDO and NPGO modes. As the different dominant mode of SST in the Northeast Pacific, the NPGO index is plotted inversely for comparison with the PDO in general. In Figure 9, negative relationships between NPGO and PDO can be observed clearly after 1986; however, the relationships between the two were obscure before 1986. Therefore, the phase relationship between NPGO and PDO is complicated. For instance, during 1986–2015, the two parameters were strongly negatively correlated (in phase). In this period, the impacts of PDO and NPGO on the upwelling and productivity are in the same direction in SBB. Indeed, significant correlations are found between NPGO, PDO, and upwelling (NPGO and upwelling: $r = 0.48$, $p < 0.001$, PDO and upwelling: $r = -0.44$, $p < 0.001$). In contrast, during 1950–1985, the two parameters were out of phase. Under such circumstances, the effects of PDO and NPGO on upwelling and productivity would be opposite; thus, in this period, there is no direct correlativity between climate indexes, and upwelling can be found. In principle, the interaction of NPGO and PDO common controls the intensity of upwelling and primary productivity, further influencing denitrification in SBB on interannual timescales.

Previous studies have found increased SST and decreased upwelling in SBB, low O_2 content in the bottom water of SBB during El Niño events, and opposite situations during La Niña events (Goericke et al., 2015; Wang et al., 2017). The O_2 content in the bottom water of SBB from California Cooperative Oceanic Fisheries Investigations (CalCOFI) during 1987–2010 is compared with our records. Furthermore, the annual upwelling record and the Niño 3.4 record are also compared with our records (Figure 9). In Figure 9, several strong El Niño events such as in 1941, 1957–1958, 1973, 1982–1983, 1997–1998, 2010, and 2016 are marked. On the annual timescale, the relationships between ENSO phases and other parameters are inconsistent; however, the comparison does appear to indicate low upwelling (hence low productivity) and high O_2 content (due to low organic consumption) corresponding to strong El Niño events, and low $\text{OC}_{\text{marine}}$ in the sediment record, e.g., 1983, 1997, and 2010, and vice versa during strong La Niña events, e.g., around 1989, 2000, and 2012. In contrast, not every equatorial El Niño affects SBB (Alfken et al., 2021). For instance, the broad $\text{OC}_{\text{marine}}$ and $\Delta\delta^{15}\text{N}_{\text{SBB}}$ peaks centered at approximately 1941 and 1994 were matched with mainly El Niño conditions, and low upwelling, $\text{OC}_{\text{marine}}$ content, and $\Delta\delta^{15}\text{N}_{\text{SBB}}$ at around 1950, 1964, and 1990 were matched with mainly La Niña conditions. In general, some strong ENSO events influence seasonal physical and biological fluctuations in SBB on the foundation of PDO and NPGO, but due to the chronology of core SBB-190629, it was used a linear sedimentation rate, and its uncertainty could be $> \pm 2$ years in some sections. The comparison can only be valid on interannual-to-decadal timescales.

5 Conclusions

The high-resolution (~0.25-year) multi-proxy analyses including TOC, TN, biomarkers, and $\delta^{15}\text{N}$ of a 46-cm sediment core (SBB-190629) collected from the SBB reveal the role of local and remote influencing factors in controlling interannual $\delta^{15}\text{N}$ variations from 1938 to 2019 CE. The $\delta^{15}\text{N}_{\text{sed}}$ records from the ETNP anoxic zone (Pescadero Slope and Soledad Basin) are further evaluated to distinctly identify the transported ETNP $\delta^{15}\text{N}$ signature and local $\delta^{15}\text{N}$ signal variability. With the use of the deviation from the mean $\delta^{15}\text{N}$ ($\Delta\delta^{15}\text{N}$) of SBB-190629 to subtract the $\Delta\delta^{15}\text{N}$ of ETNP, $\Delta\delta^{15}\text{N}_{\text{SBB}}$ fluctuations have been generated. The $\Delta\delta^{15}\text{N}_{\text{SBB}}$ reflects the bottom water denitrification, which is mainly influenced by changes in oxygen content and productivity associated with oceanic water upwelling. The comparisons between the $\Delta\delta^{15}\text{N}_{\text{SBB}}$ record and redox-sensitive multi-proxies including the Re/Mo ratio, C_{29} stanol/stenol ratio, $\text{OC}_{\text{marine}}$ content, and total marine biomarker concentration authenticate the $\Delta\delta^{15}\text{N}_{\text{SBB}}$ as an indicator of bottom water denitrification, which is proportional to marine productivity

and upwelling intensity in the SBB. In general, strong upwelling brings more nutrients and elevates marine productivity to lower O_2 content in the water column during La Niña and cold PDO conditions, resulting in high OC_{marine} and more denitrification (higher $\delta^{15}N$) and vice versa under El Niño and warm PDO. Such phenomena can be seen on annual timescales. However, the relationships of the SBB OC_{marine} and $\delta^{15}N$ records with ENSO and PDO records on longer-than-annual timescales are complicated because upwelling and O_2 content in the SBB can be influenced by PDO, NPGO, and ENSO. The combination of these climatic forcing factors has different impacts on the marine productivity in SBB at different timescales. Tropical trade winds act as a remote influencing factor and control the general trend of SBB sedimentary $\delta^{15}N$ ($\delta^{15}N_{\text{sed}}$) signature by transporting ETNP $\delta^{15}N$ signal to SBB. The general decreasing trend of the ETNP $\delta^{15}N$ from 1940 to the late 1980s probably reflected reduced upwelling, productivity, and denitrification caused by the weakening of tropical trade winds. The strength of tropical trade winds remained low during 1980–2000 and then started to increase afterward.

Data availability statement

The datasets presented in this study can be found in online repositories. The names of the repository/repositories and accession number(s) can be found in the article/[Supplementary Material](#).

Author contributions

H-CL, D-WL, and HX designed the study and wrote the paper. H-CL provided accurate dating of core SBB-190629, and HX carried out measurements on total organic carbon, total nitrogen, biomarkers, and nitrogen isotopes. All co-authors provided intellectual input for data interpretation and writing of this manuscript. All authors contributed to the article and approved the submitted version.

References

- Alfken, S., Wörmer, L., Lipp, J. S., Napier, T., Elvert, M., Wendt, J., et al. (2021). Disrupted coherence between upwelling strength and redox conditions reflects source water change in Santa Barbara basin during the 20th century. *Paleoceanogr. Paleoclimatology* 36 (12), e2021PA004354. doi: 10.1029/2021PA004354
- Alfken, S., Wörmer, L., Lipp, J. S., Wendt, J., Schimmelmann, A., and Hinrichs, K.-U. (2020). Mechanistic insights into molecular proxies through comparison of subannually resolved sedimentary records with instrumental water column data in the Santa Barbara basin, southern California. *Paleoceanogr. Paleoclimatol.* 35 (10), e2020PA004076. doi: 10.1029/2020PA004076
- Altabet, M. A. (2006). "Isotopic tracers of the marine nitrogen cycle: present and past.", in *Marine organic matter: biomarkers, isotopes and DNA*. ed. J. K. Volkman (Berlin, Heidelberg: Springer), 251–293.
- Altabet, M. A., Pilskaln, C., Thunell, R., Pride, C., Sigman, D., Chavez, F., et al. (1999). The nitrogen isotope biogeochemistry of sinking particles from the margin of the Eastern north pacific. *Deep-Sea Res. Part I-Oceanogr. Res. Pap.* 46, 655–679. doi: 10.1016/S0967-0637(98)00084-3
- Bograd, S. J., and Lynn, R. J. (2001). Physical-biological coupling in the California current during the 1997–99 El Niño-la niña cycle. *Geophys. Res. Lett.* 28 (2), 275–278. doi: 10.1029/2000GL012047
- Bograd, S. J., Schwing, F. B., Castro, C. G., and Timothy, D. A. (2002). Bottom water renewal in the Santa Barbara basin. *Geophys. Res.-Oceans* 107, 9–1-9-9. doi: 10.1029/2001JC001291
- Canfield, D. (2006). Models of oxic respiration, denitrification and sulfate reduction in zones of coastal upwelling. *Geochim. Cosmochim. Acta* 70, 5753–5765. doi: 10.1016/j.gca.2006.07.023
- Ceballos, L. I., Di Lorenzo, E., Hoyos, C. D., Schneider, N., and Taguchi, B. (2009). North pacific gyre oscillation synchronizes climate fluctuations in the

Funding

This study was supported by the National Natural Science Foundation of China (Grant No. 41876076) to D-WL, the National Natural Science Foundation of China (Grant No. 41630966) to MZ, and grants from the Ministry of Science and Technology of Taiwan (MOST 107-2116-M-002-005, MOST 108-2116-M-002-012, MOST 109-2116-M-002-018 and MOST 110-2116-M-002-015) to H-CL.

Acknowledgments

We thank Dr. D. Burdige at Old Dominion University and Dr. T. Komada at San Francisco State University for their coring.

Conflict of interest

The authors declare that the research was conducted in the absence of any commercial or financial relationships that could be construed as a potential conflict of interest.

Publisher's note

All claims expressed in this article are solely those of the authors and do not necessarily represent those of their affiliated organizations, or those of the publisher, the editors and the reviewers. Any product that may be evaluated in this article, or claim that may be made by its manufacturer, is not guaranteed or endorsed by the publisher.

Supplementary material

The Supplementary Material for this article can be found online at: <https://www.frontiersin.org/articles/10.3389/fmars.2022.982051/full#supplementary-material>

- Eastern and Western boundary systems. *J. Clim.* 22 (19), 5163–5174. doi: 10.1175/2009JCLI2848.1
- Chavez, F. P., Ryan, J., Lluch-Cota, S. E., and Naiquen, C. M. (2003). From anchovies to sardines and back: Multidecadal change in the Pacific ocean. *Science* 299 (5604), 217–221. doi: 10.1126/science.1075880
- Checkley, J. D. M., and Barth, J. A. (2009). Patterns and processes in the California current system. *Prog. Oceanogr.* 83 (1–4), 49–64. doi: 10.1016/j.pocean.2009.07.028
- Chenillat, F., Franks, P. J., Capet, X., Riviere, P., Grima, N., Blanke, B., et al. (2018). Eddy properties in the southern California current system. *Ocean Dyn.* 68 (7), 761–777. doi: 10.1007/s10236-018-1158-4
- Chhak, K., and Di Lorenzo, E. (2007). Decadal variations in the California current upwelling cells. *Geophys. Res. Lett.* 34 (14), L14604. doi: 10.1029/2007GL030203
- Chung, Y. C. (1973). Excess radon in the Santa Barbara basin. *Earth Planet. Sci. Lett.* 17 (2), 319–323. doi: 10.1016/0012-821X(73)90196-9
- Crusius, J., Calvert, S., Pedersen, T., and Sage, D. (1996). Rhenium and molybdenum enrichments in sediments as indicators of oxic, suboxic and sulfidic conditions of deposition. *Earth Planet. Sci. Lett.* 145 (1–4), 65–78. doi: 10.1016/S0012-821X(96)00204-X
- Davis, C. V., Ontiveros-Cuadras, J. F., Benitez-Nelson, C., Schmittner, A., Tappa, E. J., Osborne, E., et al. (2019). Ongoing increase in Eastern tropical north Pacific denitrification as interpreted through the Santa Barbara basin sedimentary $\delta^{15}\text{N}$ record. *Paleoceanogr. Paleoclimatol.* 34, 1554–1567. doi: 10.1029/2019PA003578
- Deser, C., Phillips, A. S., and Hurrell, J. W. (2004). Pacific interdecadal climate variability: Linkages between the tropics and the north Pacific during boreal winter since 1900. *J. Clim.* 17 (16), 3109–3124. doi: 10.1175/1520-0442(2004)017<3109:PICVLB>2.0.CO;2
- Deutsch, C., Berelson, W., Thunell, R., Weber, T., Tems, C., McManus, J., et al. (2014). Centennial changes in north Pacific anoxia linked to tropical trade winds. *Science* 345, 665–668. doi: 10.1126/science.1252332
- Di Lorenzo, E., Schneider, N., Cobb, K. M., Franks, P. J. S., Chhak, K., Miller, A. J., et al. (2008). North Pacific gyre oscillation links ocean climate and ecosystem change. *Geophys. Res. Lett.* 35 (8), L08607. doi: 10.1029/2007GL032838
- Emmer, E., and Thunell, R. C. (2000). Nitrogen isotope variations in Santa Barbara basin sediments: Implications for denitrification in the eastern tropical north Pacific during the last 50,000 years. *Paleoceanogr. Paleoclimatol.* 15, 377–387. doi: 10.1029/1999PA000417
- Eyssen, H. J., Parmentier, G. G., Compennolle, F. C., de Pauw, G., and Piessens-Denef, M. (1973). Biohydrogenation of sterols by eubacterium ATCC 21,408–Nova species. *Eur. J. Biochem.* 36 (2), 411–421. doi: 10.1111/j.1432-1033.1973.tb02926.x
- Garca-Reyes, M., and Largier, J. (2010). Observations of increased wind-driven coastal upwelling off central California. *J. Geophys. Res.-Oceans* 115 (C4), C04011. doi: 10.1029/2009JC005576
- Goericke, R., Bograd, S. J., and Grundle, D. S. (2015). Denitrification and flushing of the Santa Barbara basin bottom waters. *Deep-Sea Res. Part II-Top. Stud. Oceanogr.* 112, 53–60. doi: 10.1016/j.dsr2.2014.07.012
- Hendy, I. L., Napier, T. J., and Schimmelmann, A. (2015). From extreme rainfall to drought: 250 years of annually resolved sediment deposition in Santa Barbara basin, California. *Quat. Int.* 387, 3–12. doi: 10.1016/j.quaint.2015.01.026
- Horak, R. E., Ruef, W., Ward, B. B., and Devol, A. H. (2016). Expansion of denitrification and anoxia in the eastern tropical north Pacific from 1972 to 2012. *Geophys. Res. Lett.* 43, 5252–5260. doi: 10.1002/2016GL068871
- Howard, J. A. E., Jarre, A., Clark, A. E., and Moloney, C. L. (2007). Application of the sequential t-test algorithm for analysing regime shifts to the southern Benguela ecosystem. *Afr. J. Mar. Sci.* 29, 437–451. doi: 10.2989/AJMS.2007.29.3.11.341
- Hu, L., Shi, X., Guo, Z., Wang, H., and Yang, Z. (2013). Sources, dispersal and preservation of sedimentary organic matter in the yellow Sea: the importance of depositional hydrodynamic forcing. *Mar. Geol.* 335, 52–63. doi: 10.1016/j.margeo.2012.10.008
- Komada, T., Druffel, E. R. M., and Trumbore, S. E. J. (2004). Oceanic export of relic carbon by small mountainous rivers. *Geophys. Res. Lett.* 2004, 31(7):L07504. doi: 10.1029/2004GL019512
- Lamb, A. L., Wilson, G. P., and Leng, M. J. (2006). A review of coastal palaeoclimate and relative sea-level reconstructions using $\delta^{13}\text{C}$ and C/N ratios in organic material. *Earth-Sci. Rev.* 75 (1–4), 29–57. doi: 10.1016/j.earscirev.2005.10.003
- Liu, K. K., and Kaplan, I. R. (1989). The eastern tropical Pacific as a source of ^{15}N -enriched nitrate in seawater off southern California. *Limnology and Oceanography* 34 (5), 820–830. doi: 10.4319/lo.1989.34.5.0820
- Li, H.-C., Wang, J., Sun, J.-J., Chou, C.-Y., Li, H.-K., Xia, Y.-Y., et al. (2019). Study of jinchuan mire in NE China I: AMS ^{14}C , ^{210}Pb and ^{137}Cs dating on peat cores. *Quat. Int.* 528, 9–17. doi: 10.1016/j.quaint.2019.07.020
- Li, D., Zhao, M., and Chen, M. T. (2014). East Asian Winter monsoon controlling phytoplankton productivity and community structure changes in the southeastern south China Sea over the last 185 kyr. *Paleogeogr. Paleoclimatol. Paleoecol.* 414 (0), 233–242. doi: 10.1016/j.palaeo.2014.09.003
- Margolskee, A., Frenzel, H., Emerson, S., and Deutsch, C. (2019). Ventilation pathways for the north Pacific oxygen deficient zone. *Glob. Biogeochem. Cycle* 33, 875–890. doi: 10.1029/2018GB006149
- Masiello, C. A., and Druffel, E. R. (2001). Carbon isotope geochemistry of the Santa Clara river. *Glob. Biogeochem. Cycle* 15, 407–416. doi: 10.1029/2000GB001290
- Meyers, P. A. (1997). Organic geochemical proxies of paleoceanographic, paleolimnologic, and paleoclimatic processes. *Org. Geochem.* 27, 213–250. doi: 10.1016/S0146-6380(97)00049-1
- Muller, P. J. (1977). CN ratios in Pacific deep-sea sediments: Effect of inorganic ammonium and organic nitrogen compounds sorbed by clays. *Geochim. Cosmochim. Acta* 41 (6), 765–776. doi: 10.1016/0016-7037(77)90047-3
- Osborne, E. B., Thunell, R. C., Marshall, B. J., Holm, J. A., Tappa, E. J., Benitez-Nelson, C., et al. (2016). Calcification of the planktonic foraminifera globigerina bulloides and carbonate ion concentration: Results from the Santa Barbara basin. *Paleoceanogr. Paleoclimatol.* 31, 1083–1102. doi: 10.1002/2016PA002933
- Rayner, N., Parker, D. E., Horton, E., Folland, C. K., Alexander, L. V., Rowell, D., et al. (2003). Global analyses of sea surface temperature, sea ice, and night marine air temperature since the late nineteenth century. *J. Geophys. Res.-Atmos.* 108 (D14), 4407. doi: 10.1029/2002JD002670
- Rodionov, S. N. (2004). A sequential algorithm for testing climate regime shifts. *Geophys. Res. Lett.* 31 (9), L09204. doi: 10.1029/2004GL019448
- Rodionov, S., and Overland, J. E. (2005). Application of a sequential regime shift detection method to the Bering Sea ecosystem. *ICES J. Mar. Sci.* 62, 328–332. doi: 10.1016/j.icesjms.2005.01.013
- Rosenfeld, R. S., and Hellmann, L. (1971). Reduction and esterification of cholesterol and sitosterol by homogenates of feces. *J. Lipid Res.* 12 (2), 192–197. doi: 10.1016/S0022-2275(20)39529-8
- Sanchez, A., Juarez, M., Ortiz-Hernandez, M. C., and Dominguez-Samalea, Y. (2022). Variability of the oxygen minimum zone associated with primary productivity and hydrographic conditions in the Eastern north Pacific during the last 1200 years. *Deep-Sea Res. Part I-Oceanogr. Res. Pap.* 186, 103810. doi: 10.1016/j.dsr.2022.103810
- Sarno, C. T., Benitez-Nelson, C. R., Ziolkowski, L. A., Hendy, I. L., Davis, C. V., Tappa, E. J., et al. (2020). The impacts of flood, drought, and turbidites on organic carbon burial over the past 2,000 years in the Santa Barbara basin, California. *Paleoceanogr. Paleoclimatology* 35, e2020PA003849. doi: 10.1029/2020PA003849
- Schubert, C. J., and Calvert, S. E. (2001). Nitrogen and carbon isotopic composition of marine and terrestrial organic matter in Arctic ocean sediments: implications for nutrient utilization and organic matter composition. *Deep-Sea Res. Part I-Oceanogr. Res. Pap.* 48, 789–810. doi: 10.1016/S0967-0637(00)00069-8
- Schubert, C., Villanueva, J., Calvert, S., Cowie, G., Von Rad, U., Schulz, H., et al. (1998). Stable phytoplankton community structure in the Arabian Sea over the past 200,000 years. *Nature* 394 (6693), 563–566. doi: 10.1038/29047
- Sigman, D. M., Granger, J., DiFiore, P. J., Lehmann, M. M., Ho, R., Cane, G., et al. (2005). Coupled nitrogen and oxygen isotope measurements of nitrate along the eastern north Pacific margin. *Glob. Biogeochem. Cycle* 19 (4), GB4022. doi: 10.1029/2005GB002458
- Sigman, D. M., Robinson, R., Knapp, A. N., van Geen, A., McCorkle, D. C., Brandes, J. A., et al. (2003). Distinguishing between water column and sedimentary denitrification in the Santa Barbara basin using the stable isotopes of nitrate. *Geochem. Geophys. Geosyst.* 4, 1–20. doi: 10.1029/2002GC000384
- Sydeaman, W., Garcia-Reyes, M., Schoeman, D., Rykaczewski, R., Thompson, S., Black, B., et al. (2014). Climate change and wind intensification in coastal upwelling ecosystems. *Science* 345, 77–80. doi: 10.1126/science.12516
- Tems, C. E., Berelson, W. M., and Prokopenko, M. G. (2015). Particulate $\delta^{15}\text{N}$ in laminated marine sediments as a proxy for mixing between the California undercurrent and the California current: A proof of concept. *Geophys. Res. Lett.* 42, 419–427. doi: 10.1126/science.1251635
- Thornton, S. F., and McManus, J. (1994). Application of organic carbon and nitrogen stable isotope and C/N ratios as source indicators of organic matter provenance in estuarine systems: evidence from the Tay estuary, Scotland. *Estuar. Coast. Shelf Sci.* 38 (3), 219–233. doi: 10.1006/ecs.1994.1015
- Thunell, R. C. (1998). Particle fluxes in a coastal upwelling zone: sediment trap results from Santa Barbara basin, California. *Deep-Sea Res. Part II-Top. Stud. Oceanogr.* 45 (8–9), 1863–1884. doi: 10.1016/S0967-0645(98)80020-9
- Thunell, R. C., and Kepple, A. B. (2004). Glacial-Holocene $\delta^{15}\text{N}$ record from the gulf of Tehuantepec, Mexico: Implications for denitrification in the eastern equatorial Pacific and changes in atmospheric N_2O . *Glob. Biogeochem. Cycle* 18, 1–12. doi: 10.1029/2002GB002028

- Van Geen, A. (2001). Baja California Coring cruise OXMZ01MV: core descriptions and CTD/Rosette data: RV Melville, Lamont-Doherty Earth Observatory, Technical Report LDEO 2001-01.
- Venrick, E. L. (2012). Phytoplankton in the California current system off southern California: Changes in a changing environment. *Prog. Oceanogr.* 104, 46–58. doi: 10.1016/j.pocan.2012.05.005
- Volkman, J. K. (1986). A review of sterol markers for marine and terrigenous organic matter. *Org. Geochem.* 9 (2), 83–99. doi: 10.1016/0146-6380(86)90089-6
- Volkman, J. K., Barrett, S. M., Blackburn, S. L., Mansour, M. P., Sikes, E. L., and Gelin, F. (1998). Microalgal biomarkers: a review of recent research developments. *Org. Geochem.* 29 (5-7), 1163–1179. doi: 10.1016/S0146-6380(98)00062-X
- Wang, Y., Hendy, I., and Napier, T. J. (2017). Climate and anthropogenic controls of coastal deoxygenation on interannual to centennial timescales. *Geophys. Res. Lett.* 44, 11,528–511,536. doi: 10.1002/2017GL075443
- Wang, Y., Hendy, I. L., and Thunell, R. (2019). Local and remote forcing of denitrification in the northeast Pacific for the last 2,000 years. *Paleoceanogr. Paleoclimatol.* 34, 1517–1533. doi: 10.1029/2019PA003577
- Ward, B. B. (2011). “Nitrification in the ocean,” in *Nitrification*, ed. B. B. Ward, D. J. Arp and M. G. Klotz (Washington, DC: American Society for Microbiology Press), 323–345.
- White, M. E., Rafter, P. A., Stephens, B. M., Wankel, S. D., and Aluwihare, L. I. (2019). Recent increases in water column denitrification in the seasonally suboxic bottom waters of the Santa Barbara basin. *Geophys. Res. Lett.* 46, 6786–6795. doi: 10.1029/2019GL082075
- Xing, L., Zhao, M., Zhang, T., Yu, M., Duan, S., Zhang, R., et al. (2016). Ecosystem responses to anthropogenic and natural forcing over the last 100 years in the coastal areas of the East China Sea. *Holocene* 26, 669–677. doi: 10.1177/0959683615618248